© 2015. Published by The Company of Biologists Ltd | Journal of Cell Science (2015) 128, 397–407 doi:10.1242/jcs.162206

RESEARCH ARTICLE

SEPT9 negatively regulates ubiquitin-dependent downregulation of EGFR

Katrin Diesenberg, Monika Beerbaum, Uwe Fink, Peter Schmieder and Michael Krauss*

ABSTRACT

Septins constitute a family of GTP-binding proteins that are involved in a variety of biological processes. Several isoforms have been implicated in disease, but the molecular mechanisms underlying pathogenesis are poorly understood. Here, we show that depletion of SEPT9 decreases surface levels of epidermal growth factor receptors (EGFRs) by enhancing receptor degradation. We identify a consensus motif within the SEPT9 N-terminal domain that supports its association with the adaptor protein CIN85 (also known as SH3KBP1). We further show CIN85–SEPT9 to be localized exclusively to the plasma membrane, where SEPT9 is recruited to EGF-engaged receptors in a CIN85-dependent manner. Finally, we demonstrate that SEPT9 negatively regulates EGFR degradation by preventing the association of the ubiquitin ligase Cbl with CIN85, resulting in reduced EGFR ubiquitylation. Taken together, these data provide a mechanistic explanation of how SEPT9, though acting exclusively at the plasma membrane, impairs the sorting of EGFRs into the degradative pathway.

KEY WORDS: SEPT9, EGFR, CIN85, Sorting, Ubiquitylation

INTRODUCTION

Human septins constitute a family of guanine-nucleotide-binding proteins comprising 13 isoforms that are differentially expressed in a cell- and tissue-specific manner. Based on sequence similarity, these isoforms have been classified into the SEPT2, SEPT3, SEPT6 and SEPT7 subgroups (Kinoshita, 2003). All isoforms contain a central GTPase domain that allows them to assemble into hetero-oligomeric complexes (Sirajuddin et al., 2007). The G-domain is flanked by N- and C-terminal extensions, which provide interfaces for association with further binding partners. Accordingly, septin filaments have been described as molecular scaffolds that orchestrate the recruitment of downstream effectors. When purified from cells and tissues, septins form rod-shaped assemblies consisting of apolar hexamers and octamers. In the hexameric state, these complexes are usually composed of SEPT7 and members of the SEPT2 and SEPT6 subgroups. Individual members of the same subgroup can substitute for each other in the SEPT2–SEPT6–SEPT7 complex (Sellin et al., 2011). Octamers from dividing non-neuronal cells additionally contain SEPT9, which occupies the terminal positions. SEPT9 might thereby allow for filament elongation or abrogate the formation of septin superstructures, depending on the length of the individual splice variant incorporated (Kim et al., 2011).

Septin complexes bind to membrane surfaces enriched in negatively charged phospholipids, such as phosphoinositides (Tanaka-Takiguchi et al., 2009). They thereby form diffusion barriers that support the compartmentalization of membranes during a broad range of cellular processes, including cell division, membrane trafficking and signal transduction (Caudron and Barral, 2009). Given the fundamental importance of these processes, it is not surprising that the misregulation of certain isoforms has been correlated with the development of diseases, including tumorigenesis and neurodegeneration (Dolat et al., 2014; Mostowy and Cossart, 2012). Depletion of SEPT9, for example, has been shown to cause cytokinetic defects (Surka et al., 2002), owing to a misregulation of the abscission machinery at the midbody (Estey et al., 2010; Kim et al., 2011). Conversely, increased protein levels of SEPT9 have been detected in several tumors (Connolly et al., 2011a; Scott et al., 2005; Stanbery et al., 2010), suggesting that elevated levels of SEPT9 might induce or support the development of cancers. However, the molecular mechanisms underlying the cell biological functions of SEPT9 remain largely obscure.

The misregulation of growth factors and their receptors, in particular that of receptor tyrosine kinases (RTKs), has been correlated with several stages of cancer progression (Witsch et al., 2010). RTK signaling depends on the number of receptors exposed at the cell surface, which in turn is under dynamic regulation (Sorkin and Goh, 2009). Hence, endocytosis and intracellular trafficking of RTKs have profound effects on signaling strength and duration (Sigismund et al., 2008). In the case of the well-studied epidermal growth factor receptor (EGFR), internalization and degradative sorting have been shown to be regulated by the E3 ubiquitin ligase Cbl (Schmidt and Dikic, 2005). At high concentrations, ligand binding triggers the recruitment of Cbl to dimerized receptors at the plasma membrane and thereby induces receptor multi- and polyubiquitylation. Whether ubiquitylation is essential to drive endocytosis is still a matter of debate. However, at the level of endosomes, ubiquitin moieties are believed to support sorting of EGFR into the degradative pathway in an ESCRT-dependent manner (Haglund et al., 2003; Lu et al., 2003).

Cbl-interacting protein of 85 kDa (CIN85, also known as SH3KBP1) is an adaptor protein involved in the downregulation of RTKs such as EGFR. This function depends on its interaction with Cbl (Petrelli et al., 2002; Soubeyran et al., 2002; Szymkiewicz et al., 2002). CIN85 encodes three SH3-domains, which confer binding to atypical proline-arginine motifs (Kowanetz et al., 2003), a proline-rich middle domain and a C-terminal coiled-coil region implicated in membrane association

Leibniz-Institut für Molekulare Pharmakologie (FMP), Robert-Rössle-Straße 10, 13125 Berlin, Germany.

*Author for correspondence (krauss@fmp-berlin.de)

Received 21 August 2014; Accepted 24 November 2014

Journal of Cell Science (2015) 128, 397–407 doi:10.1242/jcs.162206

(Zhang et al., 2009). Here, we show that SEPT9, by associating with CIN85 SH3 domains, negatively regulates ubiquitin-dependent EGFR degradation, thereby linking the molecular activity of SEPT9 to cellular growth control.

RESULTS

SEPT9 controls EGFR degradation

Given the fundamental role of SEPT9 during development and its involvement in cell division and differentiation (Estey et al., 2010; Füchtbauer et al., 2011), we set out to investigate potential changes in surface levels of growth factor receptors upon RNA interference (RNAi)-mediated depletion of SEPT9. We quantified surface EGFR by applying Alexa-Fluor-647–EGF (AF647–EGF) in the cold. Strikingly, SEPT9-, but not SEPT7-depleted HeLa cells displayed a near 50% reduction in EGFR surface levels when compared with control cells (Fig. 1A–C; supplementary material Fig. S1A). Knockdown of SEPT9 also slightly decreased the total levels of EGFR (supplementary material Fig. S1B). Other surface proteins, such as β1-integrin, remained unaffected (supplementary material Fig. S1C).

As these data suggest a possible role for SEPT9 in stabilizing EGFRs, we next investigated the effects of SEPT9 depletion on

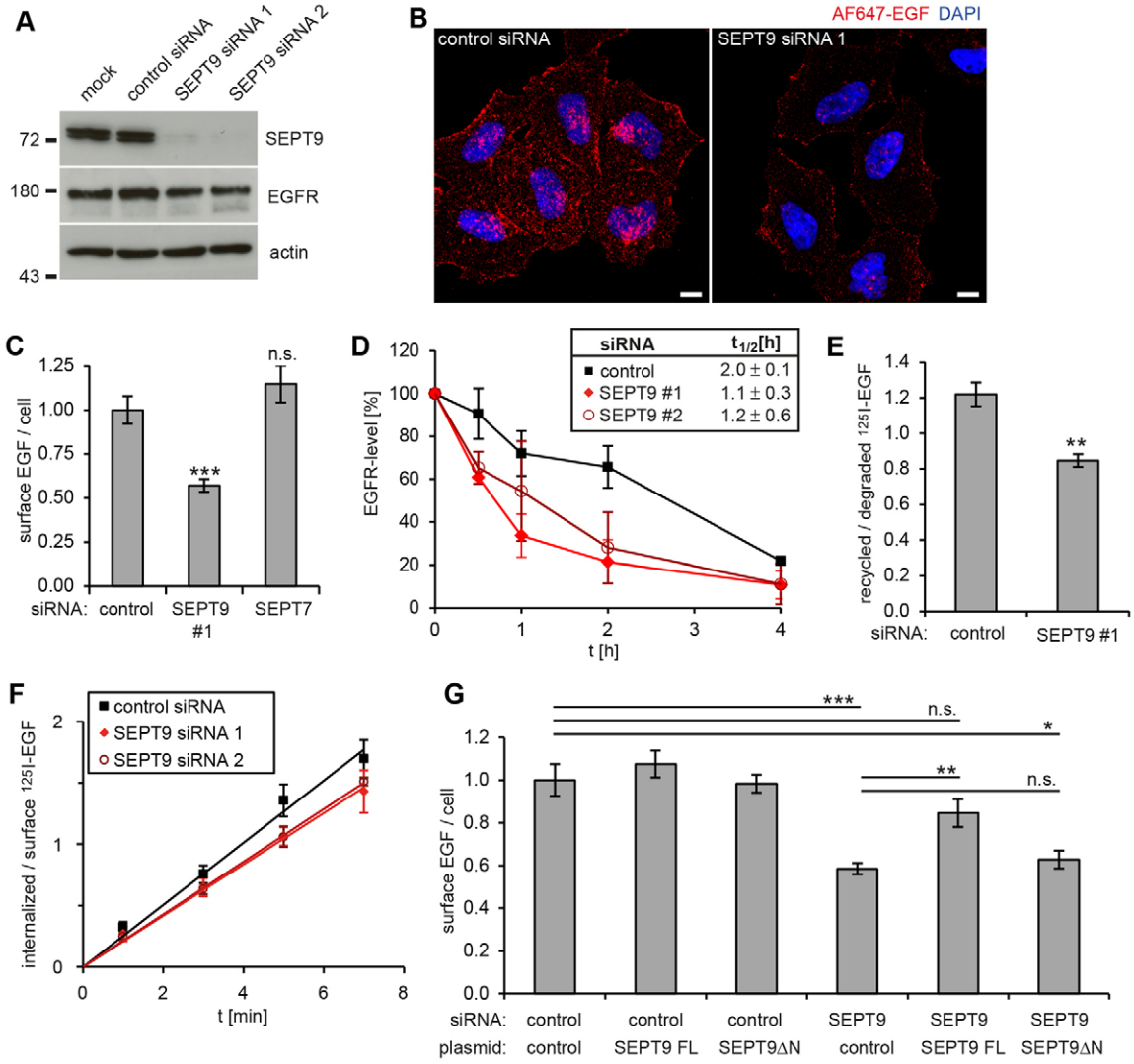

Fig. 1. SEPT9 controls endosomal trafficking of EGFR. (A) Septin siRNA verification. siRNA-treated HeLa cells were analyzed by immunoblotting using the indicated antibodies. (B,C) AF647–EGF was bound to the surface of siRNA-treated HeLa cells at 9˚C. Scale bars: 10 µm. (C) The amount of surface-bound ligand per cell was quantified by epifluorescence microscopy (n=10). (D) siRNA-treated HeLa cells were stimulated with EGF in presence of cycloheximide for the indicated times. EGFR degradation was detected by immunoblotting. $t_{1/2}$, half-lives of EGFR (n=3). (E) siRNA-treated HeLa cells were incubated with 20 ng/ml ^{125}I-EGF for 15 min and chased for 40 min. Upon recycling, intact EGF is released into the cell medium, but a minor fraction remains attached to the cell surface. Recycled ^{125}I-EGF was thus calculated as the amount of radioactivity detected in TCA precipitates from the cell medium and from an acid wash. Degraded ^{125}I-EGF reflects the amount of radioactivity found in the supernatants of TCA precipitates derived from cell medium and cell lysates. To account for differences in the level of surface EGFR, values for degraded and recycled ^{125}I-EGF were normalized to total internalized ^{125}I-EGF (n=3). (F) siRNA-treated HeLa cells were incubated with 1.5 ng/ml ^{125}I-EGF at 37˚C for the indicated times. Surface-bound ^{125}I-EGF was removed by an acid wash and quantified. The amount of internalized ^{125}I-EGF was determined upon subsequent lysis of the cells. For each time-point, internalized ^{125}I-EGF was normalized to surface-bound ^{125}I-EGF (n=3). (G) siRNA-treated HeLa cells were retransfected after 24 h with full-length (FL) SEPT9 or an HA-tagged ΔN-mutant. After an additional 24 h, cells were analyzed as in B (n=8). All quantitative data are depicted as the mean±s.e.m. (n experiments); *P<0.05; **P<0.01; ***P<0.001; n.s., not significant.

Journal of Cell Science (2015) 128, 397–407 doi:10.1242/jcs.162206

endosomal sorting of EGFR. Loss of SEPT9 substantially accelerated receptor degradation, reflected by an approximately twofold decrease in half-lives from 2 h to 1.1 h and 1.2 h (two independent siRNAs; Fig. 1D; supplementary material Fig. S1D). Accordingly, surface levels of EGFR recovered in knockdown cells when degradative processes were blocked by the addition of both proteasomal and lysosomal inhibitors (supplementary material Fig. S1E). Next, we performed pulse-chase experiments to monitor ligand-induced sorting of EGFR into degradative or recycling pathways. In knockdown cells, a larger fraction of ^{125}I-labeled EGF was degraded after 40 min of incubation as compared with that of control cells, and fewer receptors were recycled (Fig. 1E; supplementary material Fig. S1F).

Faster degradation might be the consequence of enhanced endocytic uptake of EGFR. As the mode of EGFR endocytosis is known to depend on ligand concentration (Sigismund et al., 2005), we determined the internalization rates of EGFR when stimulated with low (Fig. 1F) and high (supplementary material Fig. S1G) doses of ligand. SEPT9 depletion affected neither clathrin-dependent nor clathrin-independent endocytosis of EGFR. Taken together, these results thus demonstrate that SEPT9 modulates degradative sorting of EGFRs at the level of endosomes without affecting receptor internalization.

SEPT9 forms a complex with the adaptor protein CIN85

To gain insight into the molecular mechanisms that might underlie the SEPT9-dependent stabilization of EGFRs, we carried out knockdown-rescue experiments. Expression of full-length SEPT9, or of a truncation mutant comprising the G-domain alone (SEPT9ΔN), did not significantly alter the levels of surface EGFR (Fig. 1G; Fig. 2A). Importantly, upon re-expression of full-length SEPT9 in a SEPT9-knockdown background, surface EGFR levels almost completely recovered, whereas SEPT9ΔN,

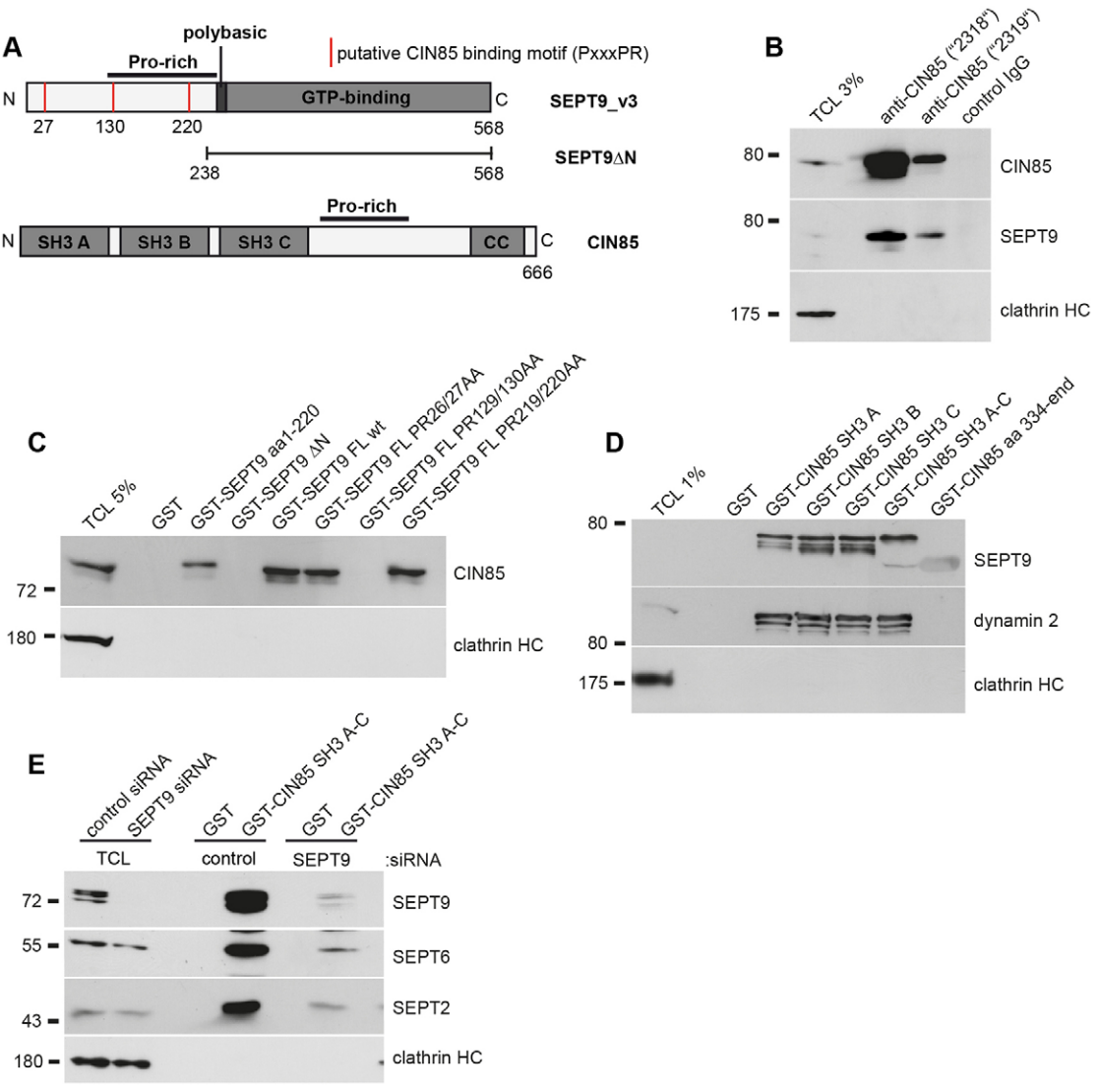

Fig. 2. SEPT9 forms a complex with CIN85. (A) Domain structure of SEPT9 transcript variant 3 (isoform c) and CIN85. A deletion variant of SEPT9 comprising the G-domain only (SEPT9ΔN) is indicated below the domain structure. (B) Two different CIN85-specific antibodies co-immunoprecipitate endogenous SEPT9 from A431 cell extracts. Precipitates were analyzed by immunoblotting with the indicated antibodies. (C–E) Affinity purification from HeLa cell extracts using the indicated GST-fused proteins as baits. Affinity-purified material was analyzed by immunoblotting with the indicated antibodies. CC, coiled-coil domain; TCL, total cell lysate; wt, wild type; FL, full length; HC, heavy chain.

Journal of Cell Science (2015) 128, 397–407 doi:10.1242/jcs.162206

the mutant lacking the N-terminal domain, was unable to restore EGFR expression. This suggests a crucial role of the SEPT9 N-terminal domain during endolysosomal sorting of EGFR.

The SEPT9 N-terminal domain is enriched in proline residues. We therefore speculated that this region might link SEPT9 to SH3-domain-containing proteins implicated in endosomal sorting and/or cytoskeletal rearrangements (supplementary material Fig. S2A). Among the various SH3 domains tested, only the three SH3 domains of CIN85 were able to retain SEPT9 from cell extracts on a glutathione-S-transferase (GST) affinity matrix. CIN85 is an adaptor protein implicated in various steps of the vesicular transport of EGFRs, including internalization, degradation and recycling (Havrylov et al., 2010), and we thus considered CIN85 as a candidate factor linking SEPT9 to EGFR sorting. We probed for a potential interaction and found a substantial fraction of endogenous SEPT9 to be co-immunoprecipitated with native CIN85 from cell extracts (Fig. 2B).

Biochemical mapping experiments revealed that the SEPT9 N-terminal domain (GST–SEPT9$_{aa1–220}$) was sufficient to promote the interaction with CIN85 (Fig. 2C; supplementary material Fig. S2C). By contrast, the isolated G-domain (GST–SEPT9ΔN) was unable to associate with CIN85. Closer inspection of the SEPT9 primary sequence revealed the presence of three atypical proline-arginine (PR) motifs in its N-terminus, which would fit the consensus sequence known to mediate interactions with CIN85 SH3 domains. (Fig. 2A) (Kowanetz et al., 2003). One particular PR motif (SEPT9 PR129/130) is highly conserved between species (supplementary material Fig. S2B). Mutational inactivation of this motif (SEPT9 PR129/130AA) almost completely abolished complex formation with CIN85, whereas the two remaining motifs (PR26/27 and PR219/220) were largely dispensable for binding. A similar binding pattern was observed when the isolated SH3 domains of CIN85 (His$_6$–CIN85 SH3A-C) were probed (supplementary material Fig. S2C), indicating that the CIN85–SEPT9 interaction is direct.

As expected, the SH3 domains derived from CIN85 were sufficient to associate with SEPT9 from cell extracts, similar to other SH3 ligands, including dynamin-2 (Schroeder et al., 2010) (Fig. 2D; supplementary material Fig. S2A). A deletion variant of CIN85 lacking the SH3 domains (CIN85 aa334-end) was unable to interact with SEPT9. Interestingly, SEPT2/6/7-containing filaments known to assemble with SEPT9 (Kim et al., 2011) were co-purified on GST-fused CIN85 SH3A-C, but only when SEPT9 was present (Fig. 2E). Collectively, our results demonstrate that an atypical PR motif links SEPT9 to the SH3 domains of CIN85. Furthermore, our data suggest that this interaction serves to recruit SEPT9-containing filaments, rather than SEPT9 monomers, to activated receptors.

CIN85 recruits SEPT9 to activated EGF receptors at the cell surface

CIN85 associates with EGFR at the level of the plasma membrane, where – together with the ubiquitin ligase Cbl – it forms part of an EGF-induced signaling complex that remains assembled during internalization and endolysosomal sorting (Haglund et al., 2002; Kowanetz et al., 2004). To investigate at which stage SEPT9 might enter this complex, we applied indirect immunofluorescence microscopy using antibodies raised against SEPT9 and CIN85 (supplementary material Fig. S3A,B; Fig. 1A). Consistent with previous reports (Surka et al., 2002), endogenous SEPT9 localized to prominent fiber-like structures positioned in close proximity to the nucleus, and to thinner filaments in the cell periphery. Overexpression of mRFP-tagged CIN85 induced the formation of enlarged, aberrant endosomes, as described previously (Zhang et al., 2009), which accumulated late-endosomal markers such as LAMP1 (supplementary material Fig. S3C) and were clearly distinct from early EEA1-containing endosomes. Importantly, overexpression of CIN85 was sufficient to trigger the relocation of endogenous SEPT9 from filamentous structures onto CIN85-positive organelles.

We then analyzed the localization of endogenous SEPT9 upon stimulation with EGF. As expected, application of EGF facilitated the recruitment of CIN85 to activated EGFRs at the surface of cells, as shown by its colocalization with AF647-labeled EGF (Fig. 3A). At these sites, CIN85 also colocalized with SEPT9 and with haemagglutinin epitope (HA)-tagged c-Cbl, a ubiquitin ligase mediating ligand-induced ubiquitylation and downregulation of EGFRs (supplementary material Fig. S3D) (Schmidt and Dikic, 2005). Of note, the degree of colocalization between SEPT9 and EGF-positive structures significantly decreased upon knockdown of CIN85 (Fig. 3B,C). A similar effect could be observed for other septin isoforms co-assembling with SEPT9, for instance SEPT2, when CIN85 was depleted (Fig. 2E; Fig. 3D). Moreover, SEPT9 depletion decreased the colocalization of SEPT2 with surface-bound EGF, supporting the idea that septin filaments are recruited to the plasma membrane in a CIN85/SEPT9-dependent manner, rather than SEPT9 mono- or multimers.

To investigate a potential role of SEPT9 during degradative sorting of EGFRs, we monitored its localization during the transport of AF647–EGF to early (5 min) and late (15 min) endosomes. SEPT9 remained associated with filaments in the cell periphery, and displayed no colocalization with internalized EGFRs, irrespective of the presence or duration of the stimulus (Fig. 4A). Furthermore, SEPT9 did not translocate to early or to recycling endosomes upon overexpression of GTP-locked eGFP–Rab5 or of wild-type eGFP–Rab11, respectively (supplementary material Fig. S4A,B). Given the functional implication of CIN85 during the assembly of the ESCRT (endosomal sorting complex required for transport) machinery (Sadoul, 2006) and the role of septins in the recruitment of ESCRT components to the site of abscission (Renshaw et al., 2014), we also considered a potential function of the SEPT9–CIN85 complex during the formation of multivesicular bodies. However, degradative endosomes stalled by overexpression of dominant negative Vps4A(E228Q) (Baumgärtel et al., 2011) (supplementary material Fig. S4C) accumulated endogenous CIN85, as expected, but not SEPT9. Collectively, these data largely exclude the possibility that a native complex of SEPT9 and CIN85 is assembled on endosomes.

Septins can associate with membrane surfaces enriched in phosphoinositides (Tanaka-Takiguchi et al., 2009). We therefore performed biochemical fractionation experiments to gain insight into the subcellular distribution of SEPT9 upon stimulation with EGF. Under these conditions (e.g. at low temperatures, when SEPT9 is not localized to filaments), we found only a small pool of SEPT9 to be associated with membranes during starvation. As anticipated, stimulation with EGF triggered the translocation of the signaling adaptor Grb-2 from the cytosol to membranes in a dose-dependent manner (Fig. 4B,C). Interestingly, the same held true for SEPT9 and its cognate binding partners SEPT2 and SEPT7. In conclusion, these results indicate that SEPT9 – though regulating degradative sorting at the level of endosomes – is transiently recruited to ligand-engaged EGFRs at the plasma membrane in a CIN85-dependent manner, but is excluded from this complex during or soon after endocytosis.

Journal of Cell Science (2015) 128, 397–407 doi:10.1242/jcs.162206

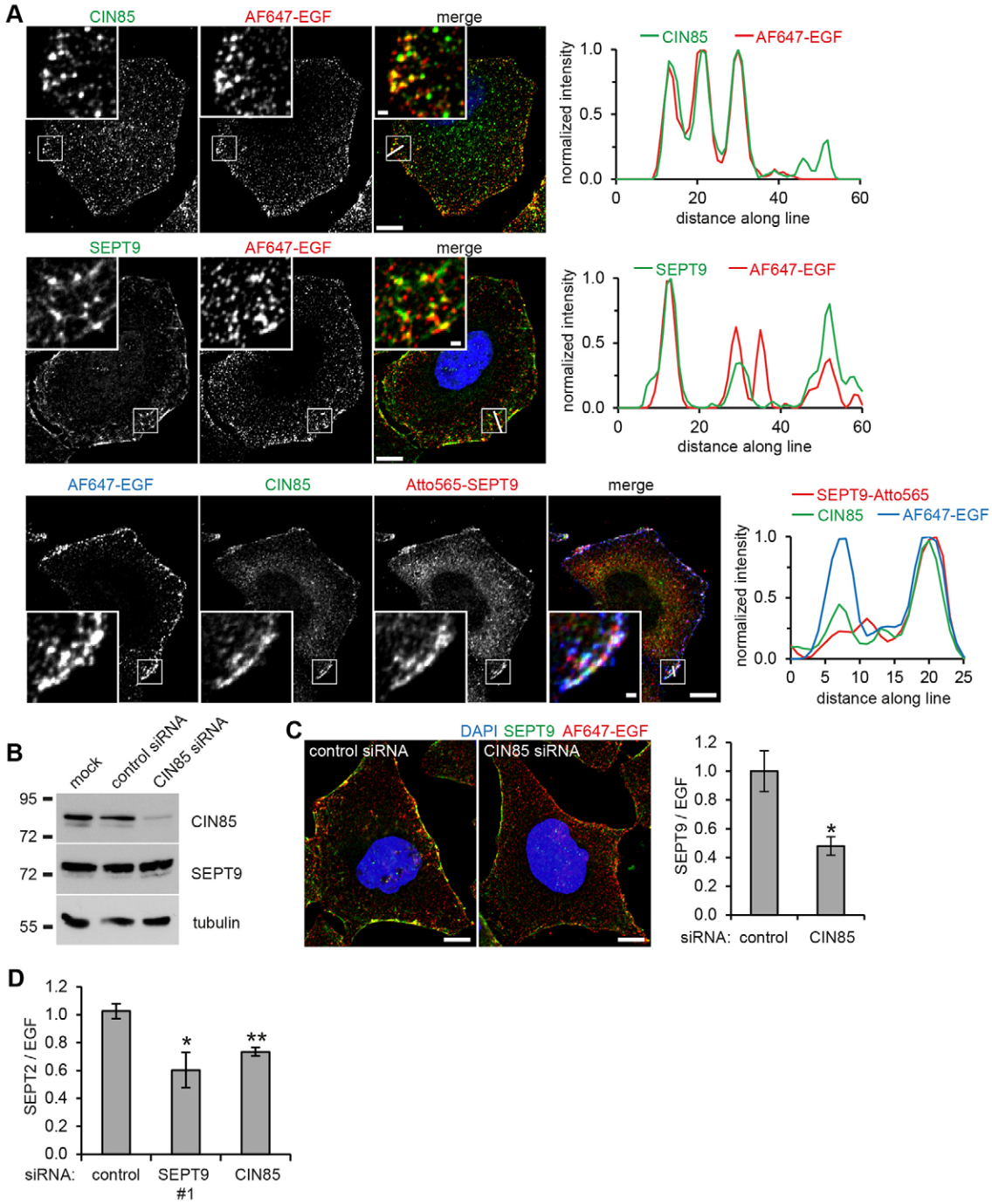

Fig. 3. SEPT9 and CIN85 partially colocalize with activated EGFR at the plasma membrane. (A) Left panels, confocal images of HeLa cells treated with 500 ng/ml AF647–EGF at 9˚C and stained for SEPT9 and CIN85. Note that SEPT9 filaments are disrupted upon treatment at low temperatures. Right panels, fluorescence intensity profiles along lines depicted in the merged images. Boxed areas are shown at higher magnification in the insets. (B) CIN85 siRNA verification. siRNA-treated HeLa cells were analyzed by immunoblotting using the indicated antibodies. (C,D) siRNA-treated HeLa cells were treated as in A and stained for SEPT9 (C) or SEPT2 (D). Scale bars: 10 µm (main images), 1 µm (insets). Colocalisation of surface-bound AF647–EGF with septin was quantified by calculating the amount of septin found in EGF-positive structures (data were corrected for total EGF bound to the cell surface) (n=3). All quantitative data are depicted as the mean±s.e.m. (n experiments); *P<0.05; **P<0.01.

Concomitant with the decrease in surface EGFR in knockdown cells, depletion of SEPT9 also significantly reduced phospho-AKT levels in cells upon stimulation with EGF (Fig. 4D; supplementary material Fig. S4D). Total AKT levels remained unaffected. By contrast, no changes in ERK1/2 signaling were detectable (supplementary material Fig S4D,E).

SEPT9 regulates Cbl-dependent ubiquitylation of EGF receptors

How can SEPT9 modulate degradative sorting of EGFR if it acts exclusively at the plasma membrane and not on endosomes? To answer this question, we followed a structure-based approach and applied nuclear magnetic resonance (NMR) spectroscopy to gain

Journal of Cell Science (2015) 128, 397–407 doi:10.1242/jcs.162206

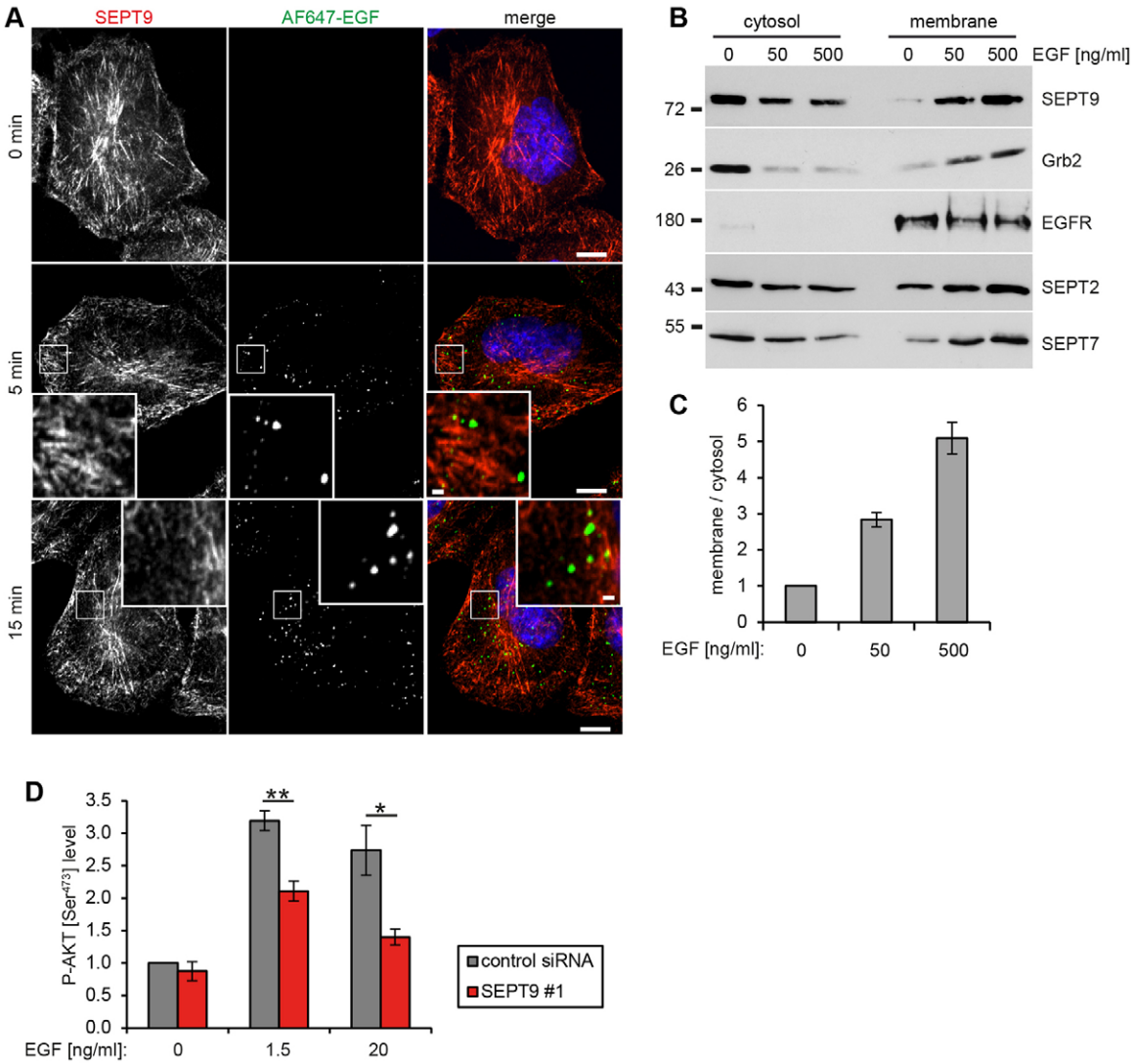

Fig. 4. Membrane recruitment of septins upon EGF stimulation. (A) Confocal images of HeLa cells upon starvation, or upon treatment with 100 ng/ml AF647–EGF at 37°C for the indicated times, stained for SEPT9. The boxed areas are shown at higher magnification in the insets. Scale bars: 10 µm (main images), 1 µm (insets). (B,C) Membrane and cytosol fractionation of EGF-stimulated HeLa cells. Equal amounts of both fractions were analyzed by immunoblotting. The ratio of membrane-associated to cytosolic SEPT9 was quantified and is shown in C (n=3). (D) siRNA-treated HeLa cells were stimulated with EGF for 5 min and subjected to ELISA to measure phospho-AKT-Ser473 level (n=3). All quantitative data are depicted as the mean±s.e.m. (n experiments). *P<0.05; **P<0.01.

insights into the molecular mechanisms underlying the association of SEPT9 with CIN85. We designed a SEPT9-derived peptide containing the PR-signature motif needed for its association with CIN85, and incubated it with the ^{15}N-labeled SH3A domain of CIN85 (Fig. 5A). Our experiments confirmed the direct association of the SEPT9 peptide with the SH3A domain of CIN85. Moreover, titration of the peptide induced changes in chemical shifts of amino acids implicated in binding to other PR-signature motifs (Fig. 5B) (Ceregido et al., 2013), indicating that both ligands compete for the same binding site. Accordingly, SEPT9- and Cbl-derived peptides occupied the same binding surface on SH3A domain of CIN85 (Fig. 5C). Affinity chromatography experiments performed in the presence of a SEPT9-derived peptide or of a mutant control peptide lacking the conserved PR-signature motif further confirmed that the binding of SEPT9 and Cbl to CIN85-SH3 domains is mutually exclusive (Fig. 5D). These structural and biochemical data suggest a molecular mechanism by which SEPT9 might regulate Cbl-mediated EGFR ubiquitylation and degradation. To test this directly, we assessed the extent of ubiquitylation of EGFRs in the presence or absence of SEPT9 upon stimulation of HeLa cells with ligand. Quantitative analyses revealed that EGFR affinity-purified from lysates of SEPT9-knockdown cells had incorporated significantly more ubiquitin than EGFR from control cells (Fig. 5E,F). These results provide a molecular explanation for the accelerated degradation observed in SEPT9-depleted cells.

DISCUSSION

Here, we identify a novel key regulatory role of SEPT9 in modulating the surface expression levels of EGFR. This function involves a highly conserved PR motif encoded by a subset of SEPT9 splice variants, which promotes the association with the SH3 domains of CIN85. SEPT9 stabilizes EGFRs by protecting them from degradation and increases the fraction of receptors

Journal of Cell Science (2015) 128, 397–407 doi:10.1242/jcs.162206

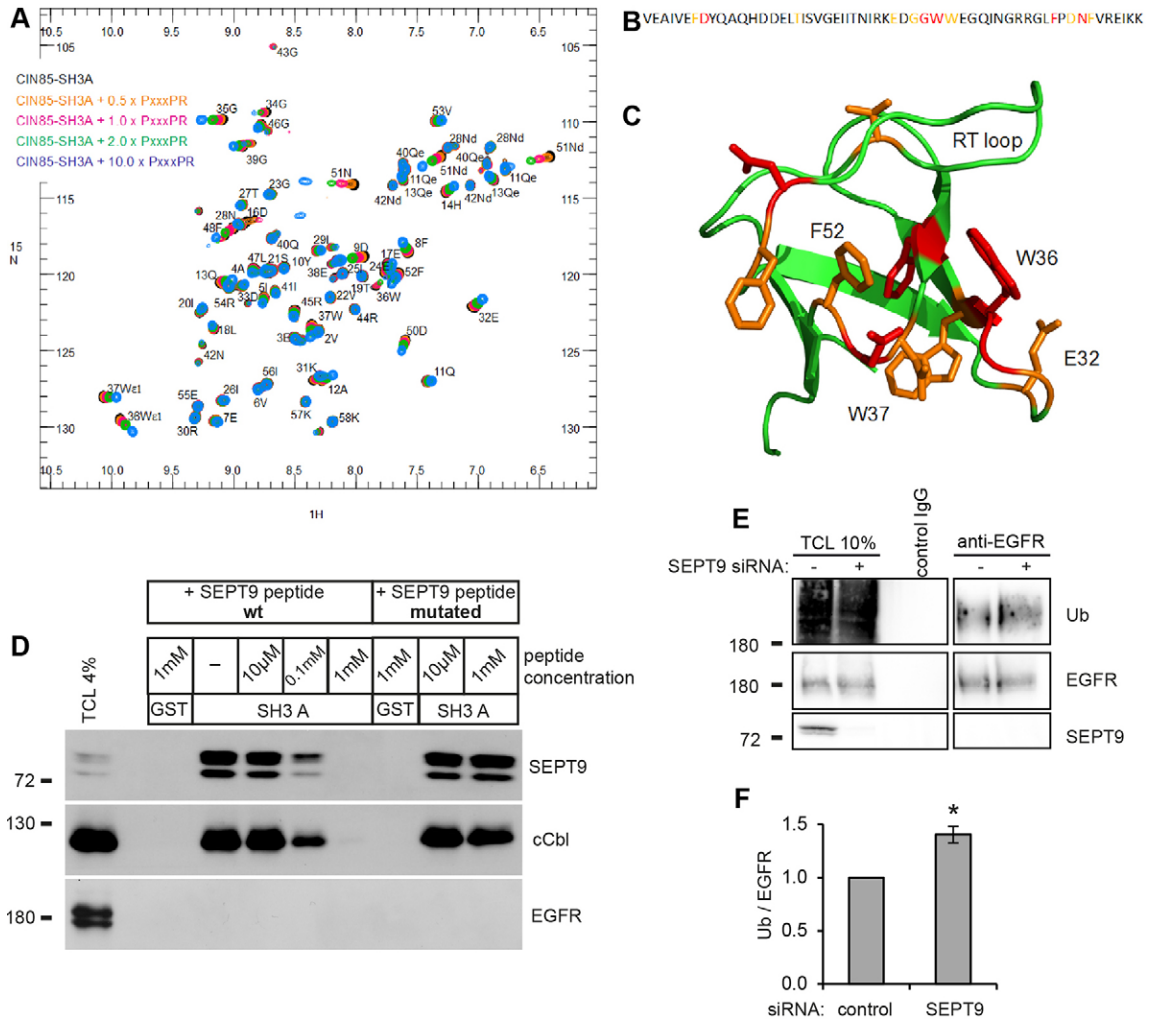

Fig. 5. SEPT9 competes with c-Cbl for binding to CIN85 and regulates EGFR ubiquitylation. (A) Overlay of the ^{1}H, ^{15}N HSQC spectra of ^{15}N-labeled CIN85 SH3 A alone with spectra from samples containing increasing amounts of the SEPT9-derived peptide PxxxPR (no peptide, 0.5×, 1×, 2×, 10× molar equivalents). The resonance assignment is shown next to the peaks. (B,C) Sequence and ribbon model of CIN85 SH3A based on the X-ray structure B2Z8. Residues for which peptide-induced chemical shift changes were observed are highlighted in red and orange. (D) HeLa cells were stimulated with 500 ng/ml EGF at 9°C and subjected to affinity purification using the SH3 A domain of CIN85 as bait. Extracts had been supplemented with a SEPT9-derived or a control peptide. (E,F) EGFR ubiquitylation in siRNA-treated HeLa cells. Cell extracts were subjected to immunoprecipitation using an EGFR-specific antibody. (F) The relative amounts of ubiquitin were quantified from n=4 experiments. TCL, total cell lysate. Data show the mean±s.e.m.; *P<0.05.

recycling back to the plasma membrane, without affecting receptor internalization. However, despite its involvement in degradative sorting, SEPT9 does not act at the level of endosomes. Instead, EGF stimulation triggers the recruitment of SEPT9 exclusively to the plasma membrane, dependent on the presence of CIN85. Finally, we demonstrate that SEPT9 competes with Cbl for binding to CIN85 and inhibits ubiquitylation of EGFRs in cells. Taken together, our data thus provide a molecular explanation for the observed effects of SEPT9 depletion on EGFR sorting.

CIN85 recruits SEPT9 to activated EGF receptors at the cell surface

CIN85 is known to remain associated with activated EGFRs during endosomal sorting (Haglund et al., 2002). Our observations suggest that SEPT9 joins this complex transiently, and is released during or soon after internalization. Based on our fractionation assays, we hypothesize that phosphatidylinositol 4,5-bisphosphate [PI(4,5)P_2] and phosphatidylinositol (3,4,5)-trisphosphate [PI(3,4,5)P_3] accumulating in the vicinity of stimulated EGFRs might aid the initial recruitment of SEPT9-containing filaments to the plasma membrane and support their retention at the cell surface (Tanaka-Takiguchi et al., 2009). According to our rescue experiments, CIN85-associated septin filaments need to contain long isoforms of SEPT9 to protect EGFRs from degradation (Fig. 1G). Of note, long SEPT9 isoforms have been shown to be upregulated in various tumors and cancer cell lines (Amir et al., 2010; Connolly et al., 2014; Connolly et al., 2011b; Stanbery et al., 2010). It remains to be determined whether and to what extent their interaction with CIN85 might contribute to cancer progression.

SEPT9 can bind to SEPT2–SEPT6–SEPT7 complexes in a non-stoichiometric manner, whereby long isoforms of SEPT9 stabilize the formation of higher-order oligomers (Kim et al., 2011). Interestingly, in comparison to members of other septin classes, SEPT9 shows the fastest hydrolysis rate (Zent and

Journal of Cell Science (2015) 128, 397–407 doi:10.1242/jcs.162206

Wittinghofer, 2014). As filament formation and stability additionally depend on the nucleotide-binding state of individual septin monomers, it is possible that interactions with the N-terminal region could affect the GTPase activity of SEPT9 in filaments and thereby induce a remodeling of local septin structures.

Septin filaments assembled in close proximity to active EGFRs could initiate the formation of a diffusion barrier, which would aid the retention of signaling complexes in subdomains of the plasma membrane (Caudron and Barral, 2009). Moreover, these filaments might serve as scaffolds that recruit further binding partners of the SEPT9 N-terminal domain or of other septin isoforms co-assembled in the same complex (Hall and Russell, 2012). For example, the SEPT9 N-terminal domain binds to a RhoA-specific guanine nucleotide exchange factor (Nagata and Inagaki, 2005), potentially allowing for crosstalk between septin filaments and the actin cytoskeleton. Several studies have further highlighted the functional interplay between septins and other elements of the cytoskeleton (Mostowy and Cossart, 2012). However, whether such local crosstalk between different components of the cytoskeleton might contribute to the modulation of EGFR trafficking remains an open question.

SEPT9 regulates Cbl-dependent ubiquitylation of EGF receptors

Our structural and biochemical data further suggest that SEPT9 competes with c-Cbl for complex formation with CIN85, thereby attenuating receptor ubiquitylation. SEPT9-sensitive ubiquitylation does not significantly affect clathrin-dependent or clathrin-independent pathways of EGF internalization, in line with the observation that several mechanisms act in a cooperative manner during EGFR endocytosis (Goh et al., 2010). Ubiquitylation, however, has an essential role during EGFR degradation (Huang et al., 2006). For instance, it has been shown that ubiquitylated EGFR associates with HRS, a component of the ESCRT-0 complex (Sigismund et al., 2005). Furthermore, perturbing the interaction between HRS and the ESCRT-I subunit Tsg101 (Lu et al., 2003), or depleting Tsg101 by RNAi (Hislop et al., 2004), attenuates EGFR degradation. Taking these observations into account, we hypothesize that SEPT9 limits the extent of EGFR ubiquitylation at the level of the plasma membrane, and thereby negatively regulates the ubiquitin-dependent association of EGFR with the ESCRT machinery at the level of endosomes. We note that CIN85 has recently been implicated in recycling of EGFRs (Schroeder et al., 2010). However, a direct role of SEPT9 in this process is unlikely, given that we found no evidence for the localization of SEPT9 on recycling endosomes (supplementary material Fig. S4B).

Besides c-Cbl/Cbl-b, numerous other factors have been found to associate with the SH3 domains of CIN85 (Buchse et al., 2011; Kowanetz et al., 2004), including proteins involved in EGFR signaling and subcellular trafficking. It is not unlikely that SEPT9 also regulates the formation of those complexes, at least as far as they are assembled at the plasma membrane, and thereby serves to coordinate their activities in time and space. Whether and how SEPT9 modulates the composition of the EGFR interactome will be subject of future studies. CIN85 and its paralog CD2AP have not only been implicated in the regulation of the surface levels of EGFR, but also of other receptor tyrosine kinases, such as c-Met (Petrelli et al., 2002). Interestingly, several septins, including SEPT9, are recruited to stimulated Met during invasion of *Listeria* and *Shigella* into HeLa cells (Mostowy et al., 2009). Moreover, the subsequent entry of bacteria appears to depend on CIN85, as well as Cbl-mediated ubiquitylation of Met (Veiga and Cossart, 2005). Whether SEPT9 regulates CIN85 function during this process as well remains to be determined.

In general, the deregulation of growth factors and their receptors is known to promote cancer progression at various stages (Witsch et al., 2010). It is interesting to note that the reduced levels of surface EGFR in SEPT9-knockdown cells correlate with reduced levels of phospho-AKT detectable upon stimulation with EGF. By contrast, phospho-ERK1/2 levels remained unchanged, indicating additional functions of SEPT9 in fine-tuning EGFR signaling. Given the role of $PI(3,4,5)P_3$ during cellular migration, this suggests that SEPT9 might modulate the migratory potential of cancer cells. In line with this hypothesis, cultured embryonic fibroblasts derived from conditional SEPT9-knockout mice have been shown to migrate more slowly than wild-type cells (Füchtbauer et al., 2011). Also in this regard, our study provides a novel molecular explanation for the genetic association of SEPT9 with cancer (Connolly et al., 2011a).

MATERIALS AND METHODS

Plasmids

Full-length and deletion variants of human SEPT9_v3 (BC021102; isoform c) and human CIN85_v1 (BC015806) were cloned into pGEX (Amersham Biosciences) or pET28a+ (Novagen) for bacterial expression or a pcDNA3-based plasmid encoding an in-frame fusion with HA, EGFP or mRFP tags for expression in mammalian cells. Site-directed mutagenesis was performed by overlapping PCR. All constructs were verified by dsDNA sequencing (MWG, BioTez). The following truncations of CIN85 were used in this study: SH3 A (amino acids 1–69), SH3 B (amino acids 96–163), SH3 C (amino acids 256–333), SH3 A-C (amino acids 1–333), C-terminal region (amino acids 334–end). The following truncations of SEPT9 were used in this study: N-terminal region (amino acids 1–220), ΔN (amino acids 238–end). For rescue experiments, an siRNA-resistant, untagged version of SEPT9 was generated.

Chemicals and antibodies

Human EGF was purchased from Peprotech. Mouse Alexa-Fluor-647-conjugated (AF647)–EGF was purchased from Life Technologies. ^{125}I-EGF for uptake experiments was obtained from Bachem (H-7112) and for recycling experiments was obtained from Perkin Elmer (NEX42800). MG132 was obtained from Calbiochem and dissolved in DMSO. NH_4Cl was obtained from Roth and dissolved in water.

For immunofluorescence experiments, antibodies were used against HA (clone HA.11, Babco/Convance), EEA1 (BD transduction, #610456), β1-integrin (EMD Millipore, #MAB1981), EGFR (clone R-1, Santa Cruz, #sc-101) and LAMP-1 (BD Pharmingen, #555801). For western blotting experiments, antibodies were used against β-actin (clone AC-15, Sigma), clathrin heavy chain (clone TD.1), dynamin 2 (BD Bioscience, #610245), c-Cbl (BD transduction, #610441), EGFR (Cell signaling, #4267), tubulin (Sigma, #T5168), ubiquitin (clone P4D1, Cell Signaling, #3936), SEPT6 (Sigma, #HPA005665), SEPT2 (Sigma, #HPA018481), Grb2 (BD Transduction, #610112), AKT1/2/3 (Cell Signaling, #9272), phospho-AKT-Ser473 (Cell Signaling, clone D9E, #4060), ERK1/2 (Abcam, #ab17942), phospho-ERK1/2 (Sigma, #M8159) and His_6-tag (Novagen, #70796-3). Quantification from western blots was performed using the western blot plugin from ImageJ.

Polyclonal antibodies against SEPT7, SEPT9 and CIN85 were raised in rabbits by injecting two different peptides. All antisera were affinity-purified and tested for specificity. For the SEPT7 antibody, rabbits were immunized against the peptide NH_2-CYEFPETDDEEENKLV-COOH. For the SEPT9 antibody, the peptides NH_2-CSTQKFQDLGVKNSEP-$CONH_2$ and NH_2-CTELSIDISSKQVEN-$CONH_2$ were co-injected. The epitope was designed such that the resulting antibody detects all long

isoforms of SEPT9 (v1, v2, v3 and v8) that contain the PR motif located at position 129-130 of isoform v3. This antibody was used throughout the whole study for immunofluorescence and immunoblotting, but not for the coimmunoprecipitation experiment in Fig. 2A. Here, the SEPT9 antibody from Abnova (H00010801-M01) was used. To allow for parallel detection of endogenous CIN85 and SEPT9, our SEPT9-specific antibody was directly coupled to Atto565 using the Lightning Link™ Rapid Conjugation System (Innova Biosciences, #351-0010) according to the manufacturer's instructions. For the generation of CIN85-specific antibodies used during immunoprecipitation, the peptides NH_2-CLQMEVNDIKKALQSK-COOH and NH_2-CKQLLSELDEEKKIRL-CONH2 were co-injected. For CIN85 antibodies used in immunofluorescence, purified His_6-tagged CIN85 (amino acids 429–end) was injected as an antigen. A CIN85 antibody from Upstate (Clone 179.1.E1) was used for immunoblotting. Secondary antibodies were purchased from Molecular Probes (conjugated to fluorescent dyes) or Dianova (horseradish peroxidase conjugated).

siRNA and peptide sequences

All siRNAs were purchased from MWG and synthesized with a 3′ TT overhang. siRNA sequences were as follows: SEPT9 #1, 5′-GGAGGAG-GUCAACAUCAAC-3′; SEPT9 #2, 5′-AGACCAUCGAGAUCAA-GUC-3′; CIN85, 5′-GGCACAGAAUGAUGAUGAA-3′; SEPT7, 5′-CUUGCAGCUGUGACUUAUA-3′; Control, 5′-AUCGUUGACUUAC-AAGAGA-3′. The sequences of the peptides used are as follows: SEPT9 PxxxPR, NH_2-EVLGHKTPEPAPRRTE-COOH; SEPT9 PxxxAA, NH_2-EVLGHKTPEPAAARTE-COOH.

Cell culture and transfection

HeLa cells (HeLa M clone) and A431 cells were grown in Dulbecco's modified Eagle's medium (Invitrogen) supplemented with 10% fetal calf serum (FCS) and antibiotics (0.1 U/ml penicillin, 0.1 µg/ml streptomycin). Plasmids were transfected into cells using JetPrime (Polyplus transfection). siRNAs were transfected into cells using Oligofectamine (Invitrogen) and the samples were analyzed after 48 h.

Immunoprecipitation

For all biochemical experiments except the EGFR ubiquitylation assay, cells were lysed in extract buffer (20 mM HEPES pH 7.4, 100 mM KCl, 2 mM $MgCl_2$, 1% Triton X-100) supplemented with 1 mM PMSF and protease inhibitor cocktail (Sigma). For experiments using EGF-stimulated cells, phosphatase inhibitor cocktails were added (Sigma, #P0044 and #P5726). Lysates were precleared by centrifugation at 13,000 ***g*** for 1 min and ultracentrifuged for 15 min at 180,000 ***g***. Extracts were incubated with antibodies immobilized on Protein-A/G-PLUS–agarose (Santa Cruz Biotechnology) for 2 h at 4℃ on a rotating wheel. Beads were washed with extract buffer and bound proteins were eluted with SDS-PAGE sample buffer.

Protein expression and purification

His_6-tagged (vector pET28a) or GST-tagged proteins (vector pGEX) were expressed in BL21 (DE3) and purified from *Escherichia coli* using His-Select Nickel Affinity Gel (Sigma) or GST Bind Resin (Novagen) according to the manufacturer's instructions.

Affinity purification on GST affinity matrices

Cell extracts were prepared as described above and incubated with purified GST-tagged proteins for 2 h at 4℃ on a rotating wheel. Beads were washed with extract buffer and bound proteins were eluted with SDS-PAGE sample buffer.

In vitro binding assay

Eluted His_6-tagged proteins were cleared from possible precipitates immediately prior to the experiment by ultracentrifugation at 180,000 ***g***. A total of 115 pmol of GST-tagged proteins was incubated with equimolar amounts of His_6-tagged proteins for 30 min at 4℃ on a rotating wheel. Beads were washed with extract buffer and bound proteins were eluted with SDS-PAGE sample buffer. During binding and washing, 10 mM imidazole was added.

NMR spectroscopy

For NMR studies, ^{15}N-labeled His_6–CIN85 SH3A (amino acids 1–58, subcloned into pET28a) was purified in 20 mM Tris-HCl pH 8, 50 mM NaCl and subjected to thrombin cleavage overnight at 4℃. The His_6-tag was removed by gel filtration on a Superdex 75 (GE Healthcare). Purified SH3A was dialyzed overnight into a buffer containing 50 mM cacodylate pH 7.4. A reference assignment of the resonances of the ^{1}H, ^{15}N-HSQC of the protein was kindly provided by others (Ceregido et al., 2013). Because the protein construct used here slightly differed from the one documented previously, we performed measurements to confirm the assignment of the protein resonances. A sample of 600 µl of ^{15}N-labeled 120 µM SH3-A was used in a 5-mm NMR tube at a temperature of 298 K. Experiments were performed on a AV600 Bruker spectrometer (600 MHz 1H frequency) using a QXI probe equipped with a self-shielding z-gradient. Three 3D experiments were performed: a ^{15}N-NOESY-HSQC using 16 scans, a data size of $512(^1H)\times64(^{15}N)\times80(^1H)$ complex points, $t_{H,max}$=51.2 ms, $t_{N,max}$=21.2 ms and $t_{H,max}(i)$=9.6 ms; a ^{15}N-TOCSY-HSQC using eight scans, a data size of $512(^1H)\times64(^{15}N)\times80(^1H)$ complex points, $t_{H,max}$=51.2 ms, $t_{N,max}$=21.2 ms and $t_{H,max}(i)$=9.6 ms; and a HNHA using eight scans, a data size of $512(^1H)\times48(^{15}N)\times46(^1H)$ complex points, $t_{H,max}$=51.2 ms, $t_{N,max}$=15.9 ms and $t_{H,max}(i)$=10.6 ms.

NMR experiments to study the interaction with a SEPT9-derived peptide were performed on a AV600 Bruker spectrometer (600 MHz ^{1}H frequency) using a TCI cryoprobe equipped with a self-shielding z-gradient. For the titration, the peptide was added from a stock solution of 5 mM or 50 mM for the higher concentrations to avoid dilution of the sample. Five ^{1}H,^{15}N-HSQCs were recorded using four scans, a data size of 512(1H)*128(15N) complex points and a $t_{H,max}$=51.2 ms and $t_{N,max}$=42.5 ms. The protein:peptide ratio was 1:0, 1:0.5, 1:1, 1:2 and 1:10. No attempt was made to completely saturate the protein. Differences in chemical shift were calculated from the peak positions in the individual spectra using the formula $\text{shift}=\text{sqrt}[(\Delta\delta(^1H))^2+(\Delta\delta(^{15}N)/10)^2]$, where $\Delta\delta$ is the difference in chemical shift in the respective dimensions.

All spectra were recorded and processed using topspin 3.1. (Bruker Biospin, Karlsruhe, Germany). The processed data were first converted to UCSF format (Goddard and Kneller, SPARKY 3. University of California, San Francisco) and subsequently transferred to CCPN (Vranken et al., 2005) for assignment. A molecular model was created using the X-ray structure B2Z8 by replacing the amino acid side chains and minimizing the energy using Sybyl.

EGFR degradation

HeLa cells were starved for 4 h in serum-free medium and incubated for the indicated times with 500 ng/ml EGF in presence of 10 µg/ml cycloheximide. For harvesting, cells were placed on ice, washed once with ice-cold PBS and scraped in extract buffer. Lysates were centrifuged for 5 min at 13,000 ***g*** and supernatants were subjected to western blot analysis. EGFR levels were quantified, corrected to a loading control (actin or tubulin) and each timecourse was normalized to time-point zero.

Immunofluorescence microscopy

Cells were seeded on Matrigel-coated coverslips and fixed with 4% paraformaldehyde (PFA), 4% sucrose in PBS for 10 min or with methanol for 5 min at −20℃. Standard protocols were used for immunostaining. For immunostaining of surface proteins, blocking and antibody decoration was performed in medium containing 10% FCS and PBS was used for washing. Images were acquired on a Zeiss Axiovert 200M-based spinning-disc confocal microscope (Perkin Elmer Inc.) under the control of Volocity software (Improvision Inc.) or by epifluorescence microscopy under the control of MicroManager. Data analysis of epifluorescence data was performed with ImageJ. Quantification of confocal images was performed with Volocity.

EGF uptake

HeLa cells were seeded on Matrigel-coated glass coverslips and starved for 3 h in serum-free medium. Cells were stimulated for the indicated

Journal of Cell Science (2015) 128, 397–407 doi:10.1242/jcs.162206

times with serum-free medium containing AF647–EGF at 37℃ and washed twice with PBS containing 2 mM $MgCl_2$ at room temperature. Upon fixation with 4% PFA/4% sucrose in PBS for 10 min, cells were analyzed by confocal microscopy.

Surface binding of EGF

HeLa cells were seeded on Matrigel-coated glass coverslips and starved for 3 h in serum-free medium. Cells were incubated with 500 ng/ml AF647–EGF for 30 min at 9℃, transferred to ice and washed twice with ice-cold PBS containing 2 mM $MgCl_2$. Upon fixation with pre-cooled 4% PFA/4% sucrose in PBS for 10 min at room temperature, cells were analyzed by immunofluorescence microscopy. For quantification of surface EGF level, cells were analyzed by quantitative epifluorescence microscopy. A subtraction of the area of the DAPI staining from the surface EGF signal was needed to decrease background fluorescence. Sum fluorescence intensity per cell was then calculated and normalized to that of the control condition. For colocalization studies with surface-bound EGF, cells were analyzed by confocal microscopy. The amount of the respective protein colocalizing with surface EGF was calculated with an intersection mask. Sum fluorescence intensity of this mask was normalized to total fluorescence intensity of EGF.

EGFR ubiquitylation

HeLa cells were starved for 3 h in serum-free medium, cooled on ice and treated with 100 ng/ml EGF for 30 min at 13℃ to prevent internalization. Cells were lysed in RIPA buffer [50 mM Tris-HCl pH 7.4, 150 mM NaCl, 1 mM EDTA, 0.1% SDS, 1% Triton X-100, 1% sodium deoxycholate, 1 mM PMSF, protease inhibitor cocktail (Sigma) and phosphatase inhibitor cocktails (Sigma, #P0044 and #P5726)]. A total of 1 mg of lysates was ultracentrifuged for 15 min at 180,000 ***g*** and incubated with EGFR-antibody (sc-101) immobilized on Protein-A/G-PLUS–agarose (both Santa Cruz Biotechnology) for 2 h at 4℃ on a rotating wheel. Beads were washed with RIPA buffer and bound proteins were eluted with SDS-PAGE sample buffer and analyzed by immunoblotting. To compensate for the decrease in EGFR level in SEPT9-knockdown samples, a 1.6-fold volume of the immunoprecipitation sample was loaded onto the gel compared to the control condition. For analysis, the amounts of ubiquitin were corrected for the amount of immunoprecipitated EGFR, which was determined from parallel gels.

Membrane and cytosol fractionation

HeLa cells were starved for 3 h in serum-free medium, cooled on ice and treated with the indicated concentrations of EGF for 60 min at 13℃ to prevent internalization. Cells were scraped in 20 mM HEPES pH 7.4, 100 mM KCl, 2 mM $MgCl_2$ and cracked using a cell cracker device (HGM, Heidelberg, Germany) following three freeze-thaw cycles in liquid nitrogen. Nuclei and cell debris were discarded following centrifugation at 1000 ***g*** for 5 min. Cytosol and membranes were separated by ultracentrifugation for 1 h at 440,000 ***g***. The membrane pellet was dissolved in hot SDS-PAGE sample buffer and thoroughly homogenized. Equal amounts of both fractions were analyzed by immunoblotting.

^{125}I-EGF uptake

^{125}I-EGF uptake was performed as described previously (Kornilova et al., 1996). HeLa cells were seeded in 24-well plates and starved for 4 h in serum-free medium containing 0.1% BSA and 20 mM HEPES pH 7.4. Cells were stimulated with ^{125}I-EGF in starvation medium at 37℃ and washed twice on ice with PBS. Surface-bound ^{125}I-EGF was removed by an acid wash with 0.2 M acetic acid, 0.5 M NaCl for 5 min on ice. The acid wash (corresponding to surface-bound EGF) was collected and radioactivity was measured using a scintillation counter (HIDEX 300SL). Cells were dried at room temperature for 5 min and lysed with 1 M NaOH for 60 min. Radioactivity of the lysate was measured (corresponding to internalized EGF). Non-specific binding was measured for each time-point in the presence of a 300-fold excess of cold EGF and was subtracted from all values. The ratio of internalized to surface-bound EGF was plotted relative to time.

^{125}I-EGF recycling and degradation

^{125}I-EGF recycling was performed as described previously (Kornilova et al., 1996). HeLa cells were seeded in 24-well plates and starved for 4 h in serum-free medium containing 0.1% BSA and 20 mM HEPES pH 7.4. Cells were stimulated with 20 ng/ml ^{125}I-EGF in starvation medium for 15 min and washed twice on ice with PBS. ^{125}I-EGF remaining on the cell surface was removed by a mild acid wash (0.2 M sodium acetate, 0.5 M NaCl, pH 4.5) on ice for 3 min. To allow for endosomal progression of EGF-bound receptors, cells were washed twice with pre-warmed starvation medium and further incubated in starvation medium containing 4 µg/ml unlabeled EGF for 40 min at 37℃. Cells were placed on ice, the medium was collected and subjected to a trichloroacetic acid (TCA) precipitation (5% TCA, 0.5% BSA; overnight at 4℃). This step serves to separate recycled, intact EGF from degraded EGF released into the medium. After washing cells twice with PBS, a minor fraction of recycled EGF that remained surface bound was removed by an acid wash (0.2 M acetic acid pH 2.5, 0.5 M NaCl for 2 min on ice). The acid wash was collected and radioactivity was measured. Cells were dried at room temperature for 30 min and lysed in 1 mM NaOH for 30 min. Cell lysates were subjected to TCA precipitation as described above. TCA-precipitated (left-over internal, intact EGF) and TCA-soluble (degraded EGF) ^{125}I were separated by a centrifugation at 13,000 ***g*** for 5 min. The pellet was dissolved in 1 M NaOH, and both fractions, supernatant and pellet, were analyzed in a γ-counter (Wallac 1470 Wizard). Non-specific counts were measured for each time-point in the presence of a 300-fold excess of unlabeled EGF and were subtracted from all values.

Total internalized EGF was calculated as the sum of measured radioactivities in all fractions derived from one well and set to 100%. Radioactivity found in TCA precipitates of the medium supernatant was added to the radioactivity in the acid wash and defined as recycled EGF. Degraded EGF was determined by the sum of the radioactivity in the TCA-soluble fractions of both medium supernatant and lysate. TCA-precipitable radioactivity in the lysate was defined as leftover internalized EGF that had remained in the cell. Recycled, degraded and leftover internalized EGF were all normalized to total internalized EGF. Receptor trafficking as depicted in Fig. 1E was plotted as the ratio of recycled to degraded EGF.

EGFR downstream signaling

Phosphorylation of AKT at Ser473 was measured using the pSer473-Akt1/2 ELISA kit (Enzo Life Sciences, #ADI-900-162). HeLa cells were starved overnight in medium containing 0.1% FCS and stimulated for 5 min at 37℃ with EGF. Cells were placed on ice, washed twice with PBS and lysed on ice in 20 mM Tris-HCl pH 7.4, 500 mM NaCl, 10 mM EDTA, 1% Triton X-100, 20 mM NaF, 20 mM β-glycerophosphate, 1 mM PMSF, protease inhibitor cocktail (Sigma) and phosphatase inhibitor cocktails (Sigma, #P0044 and #P5726). Lysates were centrifuged for 5 min at 13,000 ***g*** and supernatants were used for the ELISA assay at a final concentration of 40 µg/ml, according to the manufacturer's instructions. Total levels of pSer473-Akt1/2 were determined using a standard curve, which was processed in parallel for each experiment. Values were normalized to control cells under starved conditions. Additionally, lysates were subjected to western blot analysis to control total AKT1/2/3 levels.

Statistics

Statistical analyses were performed using the unpaired *t*-test for all quantified experiments except for the data shown in Fig. 5F (EGFR ubiquitylation after knockdown of SEPT9) and supplementary material Fig. S1B (EGFR level after knockdown of SEPT9). Here, a one-sample *t*-test was used.

Acknowledgements

We thank Dr M.A. Ceregido and Dr N.A.J. van Nuland (Vlaams Instituut voor Biotechnologie, Brussels, Belgium) for the assignment of the resonances of the ^{1}H, ^{15}N-HSQC of SH3A of CIN85, Dr G. Krause (Leibniz-Institut für Molekulare Pharmakologie, Berlin, Germany) for the creation of the structural model and Dr

Hans-Georg Krausslich (Universitätsklinikum Heidelberg, Germany) for the plasmid encoding EGFP–Vps4 E228Q.

Competing interests
The authors declare no competing or financial interests.

Author contributions
All authors contributed to the design of experiments. K.D. performed biochemical, molecular biology and microscopy experiments. U.F. purified recombinant protein for NMR spectroscopy. M.B. and P.S. performed and interpreted NMR analyses. M.K. conceived, planned and oversaw the experiments. K.D., P.S. and M.K. wrote the manuscript.

Funding
This work was supported by a grant from the German research funding agency Deutsche Forschungsgemeinschaft [grant number SFB958/A11] to M.K.

Supplementary material
Supplementary material available online at
http://jcs.biologists.org/lookup/suppl/doi:10.1242/jcs.162206/-/DC1

References
Amir, S., Golan, M. and Mabjeesh, N. J. (2010). Targeted knockdown of SEPT9_v1 inhibits tumor growth and angiogenesis of human prostate cancer cells concomitant with disruption of hypoxia-inducible factor-1 pathway. *Mol. Cancer Res.* **8**, 643-652.

Baumgärtel, V., Ivanchenko, S., Dupont, A., Sergeev, M., Wiseman, P. W., Kräusslich, H. G., Bräuchle, C., Müller, B. and Lamb, D. C. (2011). Live-cell visualization of dynamics of HIV budding site interactions with an ESCRT component. *Nat. Cell Biol.* **13**, 469-474.

Buchse, T., Horras, N., Lenfert, E., Krystal, G., Korbel, S., Schumann, M., Krause, E., Mikkat, S. and Tiedge, M. (2011). CIN85 interacting proteins in B cells-specific role for SHIP-1. *Mol. Cell Proteomics* **10**, M110 006239.

Caudron, F. and Barral, Y. (2009). Septins and the lateral compartmentalization of eukaryotic membranes. *Dev. Cell* **16**, 493-506.

Ceregido, M. A., Garcia-Pino, A., Ortega-Roldan, J. L., Casares, S., López Mayorga, O., Bravo, J., van Nuland, N. A. and Azuaga, A. I. (2013). Multimeric and differential binding of CIN85/CD2AP with two atypical proline-rich sequences from CD2 and Cbl-b*. *FEBS J.* **280**, 3399-3415.

Connolly, D., Abdesselam, I., Verdier-Pinard, P. and Montagna, C. (2011a). Septin roles in tumorigenesis. *Biol. Chem.* **392**, 725-738.

Connolly, D., Yang, Z., Castaldi, M., Simmons, N., Oktay, M. H., Coniglio, S., Fazzari, M. J., Verdier-Pinard, P. and Montagna, C. (2011b). Septin 9 isoform expression, localization and epigenetic changes during human and mouse breast cancer progression. *Breast Cancer Res.* **13**, R76.

Connolly, D., Hoang, H. G., Adler, E., Tazearslan, C., Simmons, N., Bernard, V. V., Castaldi, M., Oktay, M. H. and Montagna, C. (2014). Septin 9 amplification and isoform-specific expression in peritumoral and tumor breast tissue. *Biol. Chem.* **395**, 157-167.

Dolat, L., Hu, Q. and Spiliotis, E. T. (2014). Septin functions in organ system physiology and pathology. *Biol. Chem.* **395**, 123-141.

Estey, M. P., Di Ciano-Oliveira, C., Froese, C. D., Bejide, M. T. and Trimble, W. S. (2010). Distinct roles of septins in cytokinesis: SEPT9 mediates midbody abscission. *J. Cell Biol.* **191**, 741-749.

Füchtbauer, A., Lassen, L. B., Jensen, A. B., Howard, J., Quiroga, A. S., Warming, S., Sørensen, A. B., Pedersen, F. S. and Füchtbauer, E. M. (2011). Septin9 is involved in septin filament formation and cellular stability. *Biol. Chem.* **392**, 769-777.

Goh, L. K., Huang, F., Kim, W., Gygi, S. and Sorkin, A. (2010). Multiple mechanisms collectively regulate clathrin-mediated endocytosis of the epidermal growth factor receptor. *J. Cell Biol.* **189**, 871-883.

Haglund, K., Shimokawa, N., Szymkiewicz, I. and Dikic, I. (2002). Cbl-directed monoubiquitination of CIN85 is involved in regulation of ligand-induced degradation of EGF receptors. *Proc. Natl. Acad. Sci. USA* **99**, 12191-12196.

Haglund, K., Sigismund, S., Polo, S., Szymkiewicz, I., Di Fiore, P. P. and Dikic, I. (2003). Multiple monoubiquitination of RTKs is sufficient for their endocytosis and degradation. *Nat. Cell Biol.* **5**, 461-466.

Hall, P. A. and Russell, S. E. (2012). Mammalian septins: dynamic heteromers with roles in cellular morphogenesis and compartmentalization. *J. Pathol.* **226**, 287-299.

Havrylov, S., Redowicz, M. J. and Buchman, V. L. (2010). Emerging roles of Ruk/CIN85 in vesicle-mediated transport, adhesion, migration and malignancy. *Traffic* **11**, 721-731.

Hislop, J. N., Marley, A. and Von Zastrow, M. (2004). Role of mammalian vacuolar protein-sorting proteins in endocytic trafficking of a non-ubiquitinated G protein-coupled receptor to lysosomes. *J. Biol. Chem.* **279**, 22522-22531.

Huang, F., Kirkpatrick, D., Jiang, X., Gygi, S. and Sorkin, A. (2006). Differential regulation of EGF receptor internalization and degradation by multiubiquitination within the kinase domain. *Mol. Cell* **21**, 737-748.

Kim, M. S., Froese, C. D., Estey, M. P. and Trimble, W. S. (2011). SEPT9 occupies the terminal positions in septin octamers and mediates polymerization-dependent functions in abscission. *J. Cell Biol.* **195**, 815-826.

Kinoshita, M. (2003). Assembly of mammalian septins. *J. Biochem.* **134**, 491-496.

Kornilova, E., Sorkina, T., Beguinot, L. and Sorkin, A. (1996). Lysosomal targeting of epidermal growth factor receptors via a kinase-dependent pathway is mediated by the receptor carboxyl-terminal residues 1022-1123. *J. Biol. Chem.* **271**, 30340-30346.

Kowanetz, K., Szymkiewicz, I., Haglund, K., Kowanetz, M., Husnjak, K., Taylor, J. D., Soubeyran, P., Engstrom, U., Ladbury, J. E. and Dikic, I. (2003). Identification of a novel proline-arginine motif involved in CIN85-dependent clustering of Cbl and down-regulation of epidermal growth factor receptors. *J. Biol. Chem.* **278**, 39735-39746.

Kowanetz, K., Husnjak, K., Höller, D., Kowanetz, M., Soubeyran, P., Hirsch, D., Schmidt, M. H., Pavelic, K., De Camilli, P., Randazzo, P. A. et al. (2004). CIN85 associates with multiple effectors controlling intracellular trafficking of epidermal growth factor receptors. *Mol. Biol. Cell* **15**, 3155-3166.

Lu, Q., Hope, L. W., Brasch, M., Reinhard, C. and Cohen, S. N. (2003). TSG101 interaction with HRS mediates endosomal trafficking and receptor down-regulation. *Proc. Natl. Acad. Sci. USA* **100**, 7626-7631.

Mostowy, S. and Cossart, P. (2012). Septins: the fourth component of the cytoskeleton. *Nat. Rev. Mol. Cell Biol.* **13**, 183-194.

Mostowy, S., Nam Tham, T., Danckaert, A., Guadagnini, S., Boisson-Dupuis, S., Pizarro-Cerdá, J. and Cossart, P. (2009). Septins regulate bacterial entry into host cells. *PLoS ONE* **4**, e4196.

Nagata, K. and Inagaki, M. (2005). Cytoskeletal modification of Rho guanine nucleotide exchange factor activity: identification of a Rho guanine nucleotide exchange factor as a binding partner for Sept9b, a mammalian septin. *Oncogene* **24**, 65-76.

Petrelli, A., Gilestro, G. F., Lanzardo, S., Comoglio, P. M., Migone, N. and Giordano, S. (2002). The endophilin-CIN85-Cbl complex mediates ligand-dependent downregulation of c-Met. *Nature* **416**, 187-190.

Renshaw, M. J., Liu, J., Lavoie, B. D. and Wilde, A. (2014). Anillin-dependent organization of septin filaments promotes intercellular bridge elongation and Chmp4B targeting to the abscission site. *Open Biol.* **4**, 130190.

Sadoul, R. (2006). Do Alix and ALG-2 really control endosomes for better or for worse? *Biol. Cell* **98**, 69-77.

Schmidt, M. H. and Dikic, I. (2005). The Cbl interactome and its functions. *Nat. Rev. Mol. Cell Biol.* **6**, 907-918.

Schroeder, B., Weller, S. G., Chen, J., Billadeau, D. and McNiven, M. A. (2010). A Dyn2-CIN85 complex mediates degradative traffic of the EGFR by regulation of late endosomal budding. *EMBO J.* **29**, 3039-3053.

Scott, M., Hyland, P. L., McGregor, G., Hillan, K. J., Russell, S. E. and Hall, P. A. (2005). Multimodality expression profiling shows SEPT9 to be overexpressed in a wide range of human tumours. *Oncogene* **24**, 4688-4700.

Sellin, M. E., Sandblad, L., Stenmark, S. and Gullberg, M. (2011). Deciphering the rules governing assembly order of mammalian septin complexes. *Mol. Biol. Cell* **22**, 3152-3164.

Sigismund, S., Woelk, T., Puri, C., Maspero, E., Tacchetti, C., Transidico, P., Di Fiore, P. P. and Polo, S. (2005). Clathrin-independent endocytosis of ubiquitinated cargos. *Proc. Natl. Acad. Sci. USA* **102**, 2760-2765.

Sigismund, S., Argenzio, E., Tosoni, D., Cavallaro, E., Polo, S. and Di Fiore, P. P. (2008). Clathrin-mediated internalization is essential for sustained EGFR signaling but dispensable for degradation. *Dev. Cell* **15**, 209-219.

Sirajuddin, M., Farkasovsky, M., Hauer, F., Kühlmann, D., Macara, I. G., Weyand, M., Stark, H. and Wittinghofer, A. (2007). Structural insight into filament formation by mammalian septins. *Nature* **449**, 311-315.

Sorkin, A. and Goh, L. K. (2009). Endocytosis and intracellular trafficking of ErbBs. *Exp. Cell Res.* **315**, 683-696.

Soubeyran, P., Kowanetz, K., Szymkiewicz, I., Langdon, W. Y. and Dikic, I. (2002). Cbl-CIN85-endophilin complex mediates ligand-induced downregulation of EGF receptors. *Nature* **416**, 183-187.

Stanbery, L., D'Silva, N. J., Lee, J. S., Bradford, C. R., Carey, T. E., Prince, M. E., Wolf, G. T., Worden, F. P., Cordell, K. G. and Petty, E. M. (2010). High SEPT9_v1 expression is associated with poor clinical outcomes in head and neck squamous cell carcinoma. *Transl Oncol.* **3**, 239-245.

Surka, M. C., Tsang, C. W. and Trimble, W. S. (2002). The mammalian septin MSF localizes with microtubules and is required for completion of cytokinesis. *Mol. Biol. Cell* **13**, 3532-3545.

Szymkiewicz, I., Kowanetz, K., Soubeyran, P., Dinarina, A., Lipkowitz, S. and Dikic, I. (2002). CIN85 participates in Cbl-b-mediated down-regulation of receptor tyrosine kinases. *J. Biol. Chem.* **277**, 39666-39672.

Tanaka-Takiguchi, Y., Kinoshita, M. and Takiguchi, K. (2009). Septin-mediated uniform bracing of phospholipid membranes. *Curr. Biol.* **19**, 140-145.

Veiga, E. and Cossart, P. (2005). Listeria hijacks the clathrin-dependent endocytic machinery to invade mammalian cells. *Nat. Cell Biol.* **7**, 894-900.

Vranken, W. F., Boucher, W., Stevens, T. J., Fogh, R. H., Pajon, A., Llinas, M., Ulrich, E. L., Markley, J. L., Ionides, J. and Laue, E. D. (2005). The CCPN data model for NMR spectroscopy: development of a software pipeline. *Proteins* **59**, 687-696.

Witsch, E., Sela, M. and Yarden, Y. (2010). Roles for growth factors in cancer progression. *Physiology (Bethesda)* **25**, 85-101.

Zent, E. and Wittinghofer, A. (2014). Human septin isoforms and the GDP-GTP cycle. *Biol. Chem.* **395**, 169-180.

Zhang, J., Zheng, X., Yang, X. and Liao, K. (2009). CIN85 associates with endosomal membrane and binds phosphatidic acid. *Cell Res.* **19**, 733-746.